Thermal Stability and Reactivity of Metal Halide Filled Single-Walled Carbon Nanotubes

J. S. Bendall,[†] A. Ilie,*[,†] M. E. Welland,[†] J. Sloan,[‡] and M. L. H. Green[‡]

Nanoscience, University of Cambridge, 11 J. J. Thomson Avenue, Cambridge, United Kingdom CB3 0FF and Inorganic Chemistry Laboratory, University of Oxford, South Parks Road, Oxford, United Kingdom OX1 3QR

Received: November 6, 2005; In Final Form: January 4, 2006

Thermal stability and reactivity to oxidation of several nanocomposite systems obtained by encapsulation of metal halides in single-walled carbon nanotubes are studied. Thermogravimetric analysis coupled with Raman spectroscopy allows insight into the various contributing factors, such as charge transfer, strain, and defect formation, and establishing a hierarchy of reactivity for the systems studied (AgX@SWCNTs, with X = Br, I; SWCNTs = arc discharge and HiPCO). The activation energy for oxidation decreases considerably after filling, indicating that filled nanotubes are more amenable to controlled modifications based on chemical reactivity than the originating empty nanotubes. The complete removal of the carbon shell at high temperatures does not preserve the nanowire morphology of the encapsulated halides; these are freed on surfaces in the form of nanoparticles arranged in 1D patterns. Metallic nanoparticles were obtained after hydrogen reduction of the halides, and growth of silicon nanowires in the footprint of the originating nanocomposites was demonstrated from such Co seeds. MX@SWCNTs (M = Ag, Co) can thus be used as environmentally stable nanoscale containers that allow the deliverance of catalytic nanoparticles in a prepatterned and aligned way.

Since their discovery, single-walled carbon nanotubes (SWCNTs) have been found to exhibit remarkable structural, mechanical, and electronic properties.[1] One such property is the ability to encapsulate foreign material inside their cylindrical cavity with relative ease.[2] This allows for the synthesis of one-dimensional systems, as the SWCNT template constrains the topology of the encapsulated material and stabilizes it, permitting atomically regulated structures. Theoretical[3] and experimental[4] studies indicate modifications of the electronic and mechanical properties of both the host nanotube and the guest filling material upon encapsulation, important in the development of future devices and materials.

Previous measurements on lead-oxide-filled carbon nanotubes using Raman spectroscopy have shown instability of the filled SWCNTs due to local heating of the PbO causing disintegration of the nanotube shell.[5] In this study we demonstrate that SWCNT filling with metal halides also affects the air oxidation of the carbon shell and has the effect of lowering the reaction temperature of the bulk carbon material. However, rather than the formation of nanowires after removal of the carbon shell, as was previously reported, we show that the decomposition of the carbon nanotube walls allows for nanoscale crystals from the filling material to be formed, potentially important in the fields of catalysis and surface science.

High-temperature air oxidation of nanotubes is highly enhanced in nanotubes of small diameter[6] and by defects present within the nanotube structure.[7] These defects can occur as dangling bonds, 5,7-ring defects, bends, Y-junctions, and kinks. Strain is thus an important factor in chemical reactivity, and it is possible to change the reactivity of a nanotube by mechanical deformation.[8] Here we show encapsulation is another way of affecting their reactivity, with filling-induced strain in the nanotube walls being possibly the main reason. A hierarchy of reactivity can be formed, with pristine nanotubes being the least reactive, followed by defective nanotubes and filled nanotubes with weak interaction between the filling material and the nanotube walls. The most reactive nanotubes are expected to be those where the filling interacts strongly (such as through hybridization) with the nanotube walls.[9]

Thermogravimetric analysis (TGA) has long been carried out on nanotube samples to give an indication of material purity and quantity of non-carbonaceous material present (e.g., catalyst material). Earlier work on as-prepared and purified SWCNTs has shown that burning of material in air proceeds via a two-component process, where the energy released due to the burning of the first component lowers the activation energy needed for burning of the second component.[10] This first component is thought to be a mixture of carbon nanotubes with defects, strain, and reactive ends, where the activation energy for oxidation is lower than in the case of perfect defect-free (pristine) nanotubes.[11] Additionally, nanotube walls which have picked up carbon contamination due to their high curvature will have lower activation energy for decomposition.[12] By fitting Lorentzian curves to the differential thermogravimetric (DTG) curves an indication of sample constitution can be formed; the area of each curve corresponds to the amount of that material present in the sample.

Raman spectroscopy, which relates to both the vibrational and the electronic structure of the carbon nanotubes, is also used to give further information on the charge-transfer effects within SWCNTs with encapsulated compounds.

We encapsulated metal halides inside SWCNTs as these have been shown to achieve high filling yield. One can increase the halogen size in a series, from Cl to Br to I, with the intention of comparing possible strain effects induced in the nanotubes due to altering the size of the filling inorganic compounds. This can strictly only be done if the different halides crystallize inside the nanotubes in the same crystallographic phase. For the Ag halides, one also expects weak chemical interaction between

* Corresponding author. E-mail: ai205@cam.ac.uk.
[†] Nanoscience.
[‡] Inorganic Chemistry Laboratory.

10.1021/jp056405t CCC: $33.50
Published on Web 03/11/2006

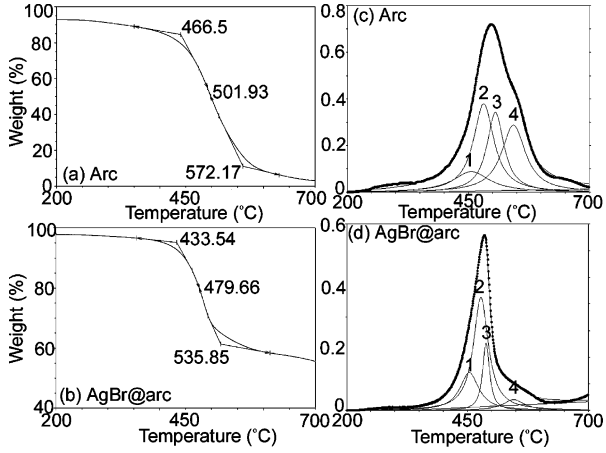

Figure 1. TGA curves of (a) purified arc SWCNTs under air/argon atmosphere at 5 °C/min heating rate and (b) AgBr@arc SWCNTs under air/argon atmosphere at 5 °C/min heating rate. Onset-, offset-, as well as midprocess temperatures[19] are indicated by the intersection of tangents to the TGA curves. DTG curves derived from the TGA curves of (c) purified arc SWCNTs and (d) AgBr@arc SWCNTs. AgBr decomposition appears in (d) as a tail with increasing slope at high temperatures.

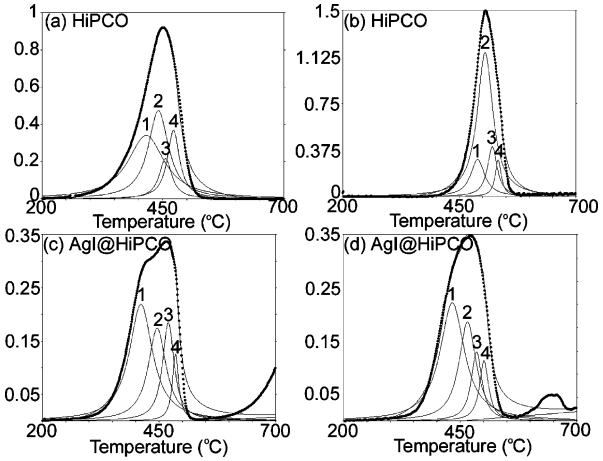

Figure 2. DTG curves of purified HiPCO SWCNTs at different heating rates under air/argon atmosphere: (a) 5 and (b) 20 °C/min. DTG curves of AgI@HiPCO SWNTs at different heating rates under air/argon atmosphere: (c) 5 and (d) 20 °C/min. After nanotube decomposition is completed, AgI decomposition starts at around 600 °C.

TABLE 1: DTG Peak Positions, Areas, and Full-Widths at Half-Maximum (fwhm) for Arc and AgBr@arc SWCNTs

	arc SWCNTs			AgBr@arc		
peak	temp (°C)	area (%)	width (°C)	temp (°C)	area (%)	width (°C)
1	455	12	69.5	453	20	44.6
2	482	32	50.7	478	59	40.7
3	506	24	44	488	13	17.3
4	543	31	63.8	548	7	60.4

the nanotube cage and the inorganic core.[9] Additionally, the covalent silver and cobalt halides can be converted to the metals relatively easily, and we used this conversion at high temperatures to free catalytic particles (such as Co) on surfaces and demonstrate subsequent silicon nanowire catalytic growth from them.

The encapsulation of silver halides in various yields[13] into SWCNTs has been previously demonstrated for both the pure halides and the AgCl−AgBr solid solution. Encapsulation is thought to occur via the opened ends of the SWCNTs, as shown by molecular dynamic simulations.[14] This behavior was also observed in the samples used for the experiments in this study, together with the apparent diameter dependence of the silver halide on filling.[15] Here the SWCNTs used for filling were either synthesized by the arc method[16] and purified by an in-house method or purchased purified from HiPCO.[17] The two methods produce a dissimilar diameter distribution, with the HiPCO SWCNTs having a distribution peak of 1 nm, fwhm of ∼0.2 nm, and the arc discharge method having a distribution peak of 1.4 nm, fwhm of ∼0.1 nm. The SWCNTs were filled using established literature methods[18] and washed to remove extraneous filling compounds. This resulted in a sample that contained predominantly nanotube species. Filling yields were about 50 ± 10% for the nanocomposites used in this study (i.e., AgBr filled inside arc nanotubes and AgI filled inside the HiPCO, as described in detail below) as determined by high-resolution transmission electron microscopy. The large error comes from variations obtained in observations made on various regions of the samples. TGA was carried out using a TA Instruments Q500 with a controlled atmosphere of 40 cm^3/min nitrogen and 60 cm^3/min dry air. Raman spectroscopy was performed on a Renishaw spectrometer using an Ar laser with a wavelength of 514.5 nm.

Figure 1a−d shows the decomposition (TGA) and corresponding DTG curves for purified arc nanotubes and silver-bromide-filled arc nanotubes (AgBr@arc). The decomposition was carried out at a slow heating rate, 5 °C/min, and in an atmosphere of dry air/N_2. This heating rate is expected to be slow relative to the speed of the C−C bond oxidation reaction.

From previous studies on the oxidation of SWCNTs peaks can be attributed to the different species present in the sample based on the DTG data. Peak 1 is assumed to be amorphous and graphitic carbons still present in the material as well as fragmented nanotubes. Peaks 2, 3, and 4, the main peaks, are assigned to several species of carbon nanotubes, going from defective to pristine by increasing the degree of perfection upon increasing the decomposition temperature. Differences occur between filled and unfilled nanotube samples: (i) a downshift in mass loss temperatures in the TGA curves upon filling, (ii) changes of peak areas, as well as (iii) significant changes in the fwhm of the DTG curves (Figure 1 and Table 1). Upon filling, while species 3 and 4 have decreased in content as reflected in significantly smaller DTG areas, species 1 and 2 have increased their contribution. Now the system is dominated by species 2, corresponding to more reactive, possibly strained, nanotubes produced as a result of filling. Notably, despite this mass redistribution, the peak positions of the Lorentzian DTG curves downshifted only a little after filling. This is also accompanied by a strong decrease of the width of the peaks, showing a stronger grouping of the filled nanotubes into the four species identified. Note that over the temperature range where decomposition takes place AgBr is expected to be in molten phase;[20,21] this might help release some of the strain that might have occurred in the solid phase.

Figure 2 and Tables 2 and 3 show similar analysis for AgI@HiPCO. Compared to AgBr@arc, in this case a potentially larger halide structure and narrower SWCNTs can combine, and thus, strain effects in the nanotube walls could be enhanced. Though the filling yield was determined to be globally similar for both AgBr@arc and AgI@HiPCO, it is expected that in the case of the narrower HiPCO nanotubes there is a cutoff diameter below which no filling can be accommodated. Two different heating rates were used: 5 °C/min (Figure 2a and c), as above for AgBr@arc, and 20 °C/min (Figure 2b and d). The relevant

TABLE 2: DTG Peak Positions, Areas, and fwhm for HiPCO and AgI@HiPCO SWCNTs at 5 °C/min Heating Rate

	HiPCO SWCNTs			AgI@HiPCO		
peak	temp (°C)	area (%)	width (°C)	temp (°C)	area (%)	width (°C)
1	415	27	85.9	410	44	66.4
2	447	57	57.7	443	28	52.2
3	463	4	38.4	464	16	26.4
4	476	9	32.6	481	11	24.4

TABLE 3: DTG Peak Positions, Areas, and fwhm for HiPCO and AgI@HiPCO SWCNTs at 20 °C/min Heating Rate

	HiPCO SWCNTs			AgI@HiPCO		
peak	temp (°C)	area (%)	width (°C)	temp (°C)	area (%)	width (°C)
1	491	22	42.5	433	49	68.6
2	506	58	42.7	466	29	48.5
3	522	15	27	485	12	31
4	534	6	16.4	501	9	27.9

characteristic data obtained from curve analysis for both the empty and AgI@HiPCO systems are shown in Tables 2 and 3.

At the slower heating rate, for both AgI- and AgBr-filled tubes the peak temperatures are very close to those of the originating species of unfilled nanotubes. These temperatures are also lower for the HiPCO-based nanocomposites than for those based on arc nanotubes, showing differences in reactivity that could be accounted for mainly by the difference in the nanotube diameter distributions. These facts demonstrate that the nature of the nanotube template did not change upon filling, i.e., a filled nanotube behaves like a defective unfilled tube rather than like a different system such as a compound of the filling with the nanotube which would be expected to have very different decomposition temperatures. This is possibly because one expects little chemical interaction between the silver atoms (with fully occupied d shells) in the silver halide and the carbon wall. The fwhm of the DTG curves is in general smaller for both types of filling (Tables 1 and 2), indicating a more homogenized distribution over the C−C bond reactivity as a result of filling. The composition of the nanotube species has altered upon filling with both halides (though the redistribution of species is different in the two cases, mainly from 4 toward 3 and 2 for AgBr@arc and from 3 and 2 toward 1 for AgI@HiPCO), showing that the defectiveness/reactivity of the nanotube walls increases as a result of filling. In the case of both filled and unfilled HiPCO-based systems, peak 1 has much higher importance relative to the other peaks than in the case of the arc-based systems. This fact can be explained if one also includes in this peak's contribution the narrowest of the HiPCO tubes; these have increased reactivity due to their strong curvature.[6] Note that based on the filling yield considerations mentioned above, peak 1 in AgI@HiPCO should have a considerable contribution from the tubes remained unfilled while filled tubes instead contribute to peaks 2−4. Furthermore, for AgI@HiPCO the decrease of the area for peak 2 of about 50% for both slow and fast heating rates could be indicative of the filling yield of the material. As this value is just for the change going from pristine to strained, the actual yield might be greater as the initially strained nanotubes would show little temperature shift upon filling. It is also a sensible value for the yield given the size of the halide and the diameter distribution of the nanotubes.

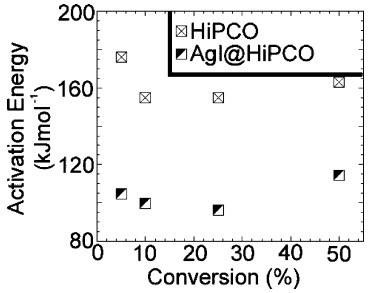

Figure 3. Activation energies for the decomposition of HiPCO and AgI@HiPCO SWCNTs at different material conversion fractions.

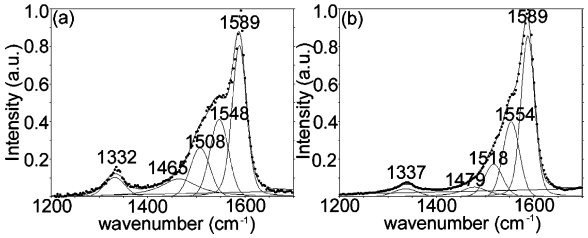

Figure 4. High-energy Raman spectra with fitting of respective peaks for (a) HiPCO SWCNTs and (b) AgI@HiPCO SWCNTs.

On increasing the heating rate of the HiPCO-based systems from 5 to 10 (not shown) and then to 20 °C/min the reaction temperature range shifts to higher temperatures (Figure 2). For the unfilled tubes there is a much stronger shift (up to 70 °C) than for AgI@HiPCO (only about 20 °C), showing that the unfilled tubes are much less reactive. There is no significant peak intensity redistribution, though their width decreases significantly, possibly due to a natural increase of the reaction rate with increasing temperature. The small upshift of the peak temperatures for AgI@HiPCO even at high heating rate is further proof of their increased reactivity: the reaction is fast enough to require only little additional thermal energy. From the TGA curves corresponding to the three heating rates the activation energy for the decomposition[22] can be determined using the Flynn−Wall−Ozawa equation[23,24]

$$\log \beta = -0.4567\left(\frac{E_a}{RT}\right) + \left(\log\left(\frac{AE_a}{R}\right) - \log F(\alpha) - 2.315\right) \quad (1)$$

Here β is the constant heating rate dT/dt, E_a the activation energy, T the absolute temperature, α the conversion fraction (i.e., the ratio between the weight of materials volatilized and the initial weight of materials), while R is the Boltzmann constant. The second term is a correction to the simply thermally activated law from the first term, where A is a preexponential factor, while $F(\alpha)$ is related to the isothermal rate of conversion $d\alpha/dt$ through the relationship $d\alpha/dt = kF(\alpha)$.[23,24] Figure 3 shows that E_a for AgI@HiPCO is lower than that for the unfilled HiPCO nanotubes by approximately 60 kJ mol^{-1}, as expected for materials with increased reactivity, and at *all* the conversion fractions (i.e., involving all the species of nanotubes in the sample, from defective to pristine). This is in agreement with previous observations, which showed that increasing the number of defective nanotubes in the system also lowers the activation energy for the burning of the pristine nanotubes.[10]

Raman spectroscopy can assist in elucidating the dominant factors that increased the reactivity of the Ag-halide-filled nanotubes. Figure 4a,b shows the tangential modes (TM) for HiPCO and AgI@HiPCO, respectively. For the HiPCO nanotubes, the TM modes resonant with 2.41 eV laser excitation

correspond mainly to metallic nanotubes. Upon filling, the G^+ band, the high-frequency part of the TM modes, remained unchanged. However, the lower frequency G^- band, sensitive to the metallic character of the nanotubes (and showing a Breit−Wigner−Fano profile),[25] became less pronounced. The three peaks composing it, at 1465, 1508, and 1548 cm^{-1}, upshift to 1479, 1518, and 1554 cm^{-1}, respectively, while their intensity and line width decrease relative to the unchanged G^+ band. The upshifts indicate a hardening of the C−C bonds, consistent with electron transfer from the nanotube walls to the AgI acceptor. This electron depletion of the nanotubes also translates to decreased electron−phonon coupling and thus a weakened Breit−Wigner−Fano profile of the G^- band, as observed in Figure 4b.

Thus, encapsulating an acceptor compound such as AgI results in charge transfer that overall hardens the C−C bonds and therefore should exhibit lower reactivity. Consequently, charge transfer to the halide is not responsible for the observed increased reactivity of AgI@SWCNTs. This leaves other factors responsible, such as an anisotropic change in the curvature of the nanotubes and defect formation. Bonds of increased curvature have been shown to induce chemical adsorption that cannot occur on flatter bonds,[8] while HRTEM observations indeed showed that anisotropic curvature changes (with changes of the nanotube cross section from circular to slightly oval or polygonized) can occur as a result of encapsulation.[26]

We can now establish a hierarchy of reactivity for the systems studied above (higher reactivity is denoted by ">")

$$\text{AgI@HiPCO} > \text{HiPCO SWCNTs} \gg \text{AgBr@arc} > \text{arc SWCNTs} \quad (2)$$

This highlights the fact that filling larger diameter nanotubes with a compound that does not bind chemically with the carbon walls does not affect the nanotube's reactivity as much as decreasing its diameter by about 0.4 nm. Also, bond hardening due to charge transfer from the nanotube cage to the acceptor halide is overcome by effects such as strain and defect formation in the nanotube walls that overall increase reactivity to oxidation. Approximate values for the nanotube diameters that would optimally accommodate AgI and AgBr in the $2 \times 2 \times \infty$ configuration can be calculated from these halides' interatomic distances in bulk phase and considering a van der Waals radius of 0.17 nm for the carbon atoms. $d_{optimum} = 1.15$ and 1.09 nm for AgI and AgBr, respectively, reflecting the larger ionic radius of I^- relative to Br^- ($r_{I^-} = 0.206$ nm, $r_{Br^-} = 0.182$ nm), while the ionic radius of Ag^+ ($r_{Ag^+} = 0.129$ nm) is smaller than both halogen ions' radii. For these estimations it was considered that both halides crystallize in the rock-salt structure: this is the usual bulk structure for AgBr,[27] while for AgI the rock-salt phase was found to occur for bulk material under high pressure (>3 kbar)[28] or, equivalently, in AgI@SWCNTs due to the pressure induced by the nanotube template during filling crystallization.[29] Thus, for AgI@HIPCO whose nanotube diameter distribution peaks around 1 nm, below $d_{optimum}$ for the AgI system, a large proportion of the nanotubes will possibly accommodate a strained, heavily puckered form of $2 \times 2 \times \infty$ AgI by analogy with the KI-filled single-walled nanotubes.[30] To accommodate such a filling in the narrow HIPCO nanotubes, the interaction between the nanotube walls and the filling is of repulsive type, which could conceivably produce stronger distortions of the nanotube walls and justify the increased reactivity observed in the AgI@HIPCO system. A direct comparison of the AgBr@arc and AgI@HIPCO systems based on induced nanotube strain is not straightforward to make. Though the $2 \times 2 \times \infty$ configuration occurs for AgBr in the arc tubes of narrower diameters (and in this case lesser strain would occur in nanotubes of same diameter when filled with AgBr as compared to when filled with AgI due to the smaller size of AgBr), it is not the one occurring in the larger arc nanotubes that makes the majority of the arc nanotube distribution peaking around 1.2 nm diameter. For larger arc nanotubes, equally larger filling configurations are to be expected,[30] so that strain effects of the nanotube walls are hard to predict and compare. A control experiment, currently under way, that would allow a more direct comparison between the filled systems involves AgBr@HIPCO; this is because AgBr in single-walled nanotubes always adopts the rock-salt phase,[27] the same as in bulk. This case is unlike that of AgI, whose stabilized phase strongly depends on the nanotube diameter: while this phase is rock salt in the narrower AgI@HiPCO, several other phases can occur in larger nanotubes, similar to the various phases possible in the bulk material, as the pressure exerted by the nanotube decreases.[28] This is supported by HRTEM observations on filled Nanocyl SWCNTs,[31] which have a diameter peak distribution around 2 nm, where the dominant crystallographic phase of AgI was found to be different.[31] Consequently, AgI@arc is not a good control system as the arc-produced nanotubes contain considerably larger tubes than HiPCO.

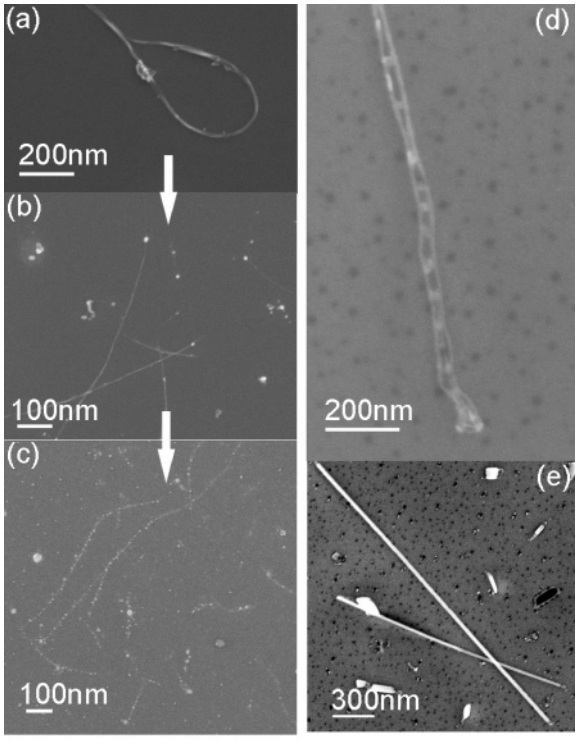

Figure 5. Evolution of AgI@HiPCO after heating in an oxidizing atmosphere at (a) 350, (b) 430, and (c) 490 °C. (d,e) Si nanowire growth from $CoCl_2$@SWNTs after decomposition and reduction showing two different morphologies.

The oxidative decomposition process was continued at higher temperatures in order to attempt to free the encapsulated inorganic nanowires on surfaces and therefore test this procedure as a method to create very thin nanowires of inorganic materials. Figure 5a−c shows stages of this process: AgBr@arc are annealed in air at increased temperatures of 350, 430, and 490 °C, respectively. At the highest temperature, there is complete decomposition of the nanotube template and AgBr is freed on the surface in form of nanoparticles and thus without preserving the one-dimensional structure as when encapsulated. This behavior is in contrast with the claim from ref 5 that PbO

nanowires could be obtained after removal of the nanotube carbon shell by laser heating in air.

Furthermore, an application of the oxidative decomposition process is to use the freed inorganic nanoparticles as catalytic seeds for the growth of other low-dimensional systems. At the temperature from Figure 5c, AgBr is in the molten phase but not decomposed or having reacted with oxygen. As shown by Raman spectroscopy, there is disordered carbon still present around the AgBr nanoparticles. These nanoparticles can then be reduced to pure metal under hydrogen flow.

Growth of nanostructures can be initiated from the resulting pure metal catalysts. In the case of Ag nanoparticles, multiwalled nanotubes could be synthesized at 850 °C from the remaining disordered carbon that acts as feedstock. Furthermore, by using a more catalytically active filling material, such as $CoCl_2$ subsequently reduced to Co, Si nanowires can be grown through a VLS process at the sites where the filled nanotubes were initially placed. In this case, as a high growth temperature (1050 °C) was used, the carbon feedstock is fully decomposed so the Co catalyzes growth directly from the Si surface. Figure 5d,e shows two different morphologies of Si nanowires that can be formed. This demonstrates that filled nanotubes can be used as environmentally stable catalyst containers. We would like to stress that we are not proposing this method as an alternative to well-established methods for the growth of nanostructures but due to its suitability for delivering catalysts in a *prepatterned* way. Catalytic nanoparticles can be freed in a 1D pattern already preformed by the nanotube template. Using various schemes that are available to align nanotubes on surfaces[32] or relative to other preexistent nanostructures, the formation of ordered one-dimensional arrays of catalytic particles could be controlled to a high degree.

In conclusion, we studied the thermal stability and reactivity to oxidation of SWCNTs filled with metal halides. A hierarchy of reactivity could be established based on the types of templating SWCNTs and filling materials. The activation energy for oxidation can decrease considerably after filling, as shown in the case of AgI@HIPCO nanocomposites. Strain and defect formation can override opposing processes, such as charge transfer resulting in C−C bond hardening, and increase the chemical reactivity of these nanocomposites relative to the originating SWCNTs. Such nanocomposites can be used as environmentally stable catalyst nanocontainers, from which aligned nanowire growth can be catalyzed at high temperatures in the foot-print of the originating nanotubes.

Acknowledgment. This work is part of an exploratory project within the Interdisciplinary Research Collaboration (IRC) in Nanotechnology, United Kingdom. A.I. and J.S.B. gratefully acknowledge funding in the form of a research grant and studentship, respectively, from the IRC.

References and Notes

(1) Terrones, M. *Annu. Rev. Mater. Res.* **2003**, *33*, 419.

(2) Meyer, R. R.; Sloan, J.; Dunin-Borkowski, R. E.; Kirkland, A. I.; Novotny, M. C.; Bailey, S. R.; Hutchison, J. L.; Green, M. L. H. *Science* **2000**, *289*, 1324.

(3) Yam, C.; Ma, C.; Wang, X.; Chen, G. *Appl. Phys. Lett.* **2004**, *85*, 4484.

(4) Ilie, A.; Bendall, J. S.; Kubo, O.; Sloan, J.; Green, M. L. H. *Phys. Rev. B*, in press.

(5) Hulman, M.; Kuzmany, H.; Costa, P. M. F. J.; Friedrichs, S.; Green, M. L. H. *Appl. Phys. Lett.* **2004**, *85*, 2068.

(6) Bom, D.; Andrews, R.; Jacques, D.; Anthony, J.; Chen, B.; Meier, M. S.; Selegue, J. P. *Nano Lett.* **2002**, *2*, 615.

(7) Lu, X.; Ausman, K. D.; Piner, R. D.; Ruoff, R. S. *J. Appl. Phys.* **1999**, *86*, 186.

(8) Gulseren, O.; Yildirim, T.; Ciraci, S. *Phys. Rev. Lett.* **2001**, *87*, 116802.

(9) Fagan, S. B.; Souza Filho, A. G.; Mendes Filho, J.; Corio, P.; Dresselhaus, M. S. *Chem. Phys. Lett.* **2005**, *406*.

(10) Rinzler, A. G.; Liu, J.; Dai, H.; Nikolaev, P.; Huffman, C. B.; Rodríguez-Macías, F. J.; Boul, P. J.; Lu, A. H.; Heymann, D.; Colbert, D. T.; Lee, R. S.; Fischer, J. E.; Rao, A. M.; Eklund, P. C.; Smalley, R. E. *Appl. Phys. A* **1998**, *67*, 29.

(11) Zhang, M.; Yudasaka, M.; Koshio, A.; Iijima, S. *Chem. Phys. Lett.* **2002**, *364*, 420.

(12) Dujardin, E.; Ebbesen, T. W.; Krishnan, A.; Treacy, M. M. J. *Adv. Mater.* **1998**, *10*, 611.

(13) Sloan, J.; Terrones, M.; Nufer, S.; Friedrichs, S.; Bailey, S. R.; Woo, H.-G.; Ruhle, M.; Hutchison, J. L.; Green, M. L. H. *J. Am. Chem. Soc.* **2002**, *124*, 2116.

(14) Wilson, M.; Madden, P. A. *J. Am. Chem. Soc.* **2001**, *123*, 2101.

(15) Sloan, J.; Wright, D. M.; Bailey, S.; Brown, G.; York, A. P. E.; Coleman, K. S.; Green, M. L. H.; Wright, D. M.; Hutchison, J. L.; Woo, H.-G. *Chem. Commun.* **1999**, 699.

(16) Journet, C.; Maser, W. K.; Bernier, P.; Loiseau, A.; Lamy De La Chapelle, M.; Lefrant, S.; Deniard, P.; Lee, R.; Fischer, J. E. *Nature* **1997**, *388*, 756.

(17) Nikolaev, P.; Bronikowski, M. J.; Bradley, R. K.; Rohmund, F.; Colbert, D. T.; Smith, K. A.; Smalley, R. E. *Chem. Phys. Lett.* **1999**, *313*, 91.

(18) Brown, G.; Bailey, S. R.; Novotny, M.; Carter, R.; Flahaut, E.; Coleman, K. S.; Hutchison, J. L.; Green, M. L. H.; Sloan, J. *Appl. Phys. A* **2003**, *76*, 457.

(19) The onset temperature (T_{onset}) is obtained by the drawing of tangents to the TG curve at the initial horizontal baseline and the steepest part of the curve and marking their intersection. The temperature when the reaction is one-half over ($T_{0.5}$) is found by curve inspection when the conversion fraction $\alpha = 0.5$. Finally, the extrapolated offset temperature (T_o) is found in a similar way to T_{onset}, just using the final baseline (In *Principles of Thermal Analysis and Calorimetry*; Haines, P. J., Ed.; Royal Society of Chemistry: London, 2002.

(20) The melting temperatures for AgBr and AgI in the bulk phase are 450 and 560 °C, respectively. These temperatures are expected to decrease when the halides form nanowires, as shown also for metallic nanowires.[21]

(21) Wang, J.; Chen, X.; Wang, G.; Wang, B.; Lu, W.; Zhao, J. *Phys. Rev. B* **2002**, *66*, 085408.

(22) Seo, M.; Park, S. *Macromol. Mater. Eng.* **2004**, *289*, 368.

(23) Flynn, J. H.; Wall, L. A. *Polym. Lett.* **1966**, *4*, 323.

(24) Ozawa, T. *Bull. Chem. Soc. Jpn.* **1965**, *38*, 1881.

(25) Brown, S. D. M.; Jorio, A.; Dresselhaus, M. S.; Dresselhaus, G. *Phys. Rev. B* **2001**, *64*, 073403.

(26) Philp, E.; Sloan, J.; Kirkland, A. I.; Meyer, R. R.; Friedrichs, S.; Hutchinson, J. L.; Green, M. L. H. *Nat. Mater.* **2003**, *2*, 788.

(27) West, A. R. *Basic Solid State Chemistry*; John Wiley & Sons, Ltd.: New York, 1999.

(28) Hanson, R. C.; Fjeldly, T. A.; Hochheimer, H. D. *Phys. Stat. Sol.* **1975**, *70*, 567.

(29) Sloan, J.; Kirkland, A. I.; Hutchinson, J. L.; Green, M. L. H. *C. R. Phys.* **2003**, *4*, 1063.

(30) Wilson, M. *Chem. Phys. Lett.* **2002**, *366*, 504.

(31) Unpublished work.

(32) Rao, S. G.; Huang, L.; Setyawan, W.; Hong, S. *Nature* **2003**, *425*, 36.